Dual Current Loop Control for a Third-Order Passive Damped Filter Based Quasi-Z-Source Inverter

Arvind Yadav[1†], **Vinay Kumar Deolia**[1], and **Sanjay Agrawal**[2], Non-members

ABSTRACT

An Impedance Source Inverter (ZSI) offers a solution to low output renewable energy sources, because it provides an unconventional high boost. The interaction of Quasi-Z-Source (qZS) inverter with the load side raises stability concerns. Multiple resonant features need attention when grid is connected. In this paper, the resonant feature of a third order filter based on a qZS inverter is explored, and DC and AC sides dynamic characteristics are analyzed for optimum size selection of passive components. Coupled response of a qZS inverter and the AC side filter is presented. For input variation, a closed loop control is established to take care of stability and the multiple resonant feature. A voltage loop and a dual current loop are used for DC and AC side dynamics respectively. Controllers are designed to mitigate input side disturbance. Results are provided for two design cases (case I, II), the need for damping is highlighted, and measured results validate the design and control methodology.

Keywords: Quasi-Z Source Inverter, Dual Current Loop, Grid Connected Inverters, LCL Filter, Passive Damping

1. INTRODUCTION

With an interfacing using a passive network between a DC source and a Voltage Source Inverter (VSI), high boost output voltage can be obtained. The first topology used was Impedance Source Inverters (ZSI) [1]. With an impedance network with only a single stage, DC-AC power conversion is possible. Many such configurations are available in literature [2–5]. The basic configuration of a ZSI network can buck/boost, draws discontinuous current, and imposes high voltage stress on passive elements [6–9]. The modification in ZSI has led to Quasi-Z-source inverters (qZSI) suitable for renewable energy application. A qZSI draws continuous current, has a reduced passive component rating, and low starting inrush current [10–12]. QZSI utilizes the energy stored in the passive components of impedance network. The presence of a capacitor and an inductor in qZSI influences the input/output transfer function. In grid tied applications, dynamic interaction of VSI, filter, and grid has been extensively explored [13–16]. Dynamic interaction of qZSI with filter and grid had been ignored in previous work, where most research work focused on DC side controller design methods, but ignored the influence on AC side [17, 18]. The behavior of qZSI is not as straight forward as that of conventional VSI. Stable operation and controller design is severely influenced by qZSI passive elements since they contribute additional resonant frequencies. The controller design for DC and AC side is mostly presented with a first or second order filter, but that neglected the double resonant feature. [19] concluded presence of additional resonant frequency compared to conventional VSI, while presenting ZSI output impedance dynamic influence for uninterrupted power supply. [20] highlighted the need for damping due to oscillatory response of current fed ZSI during dynamic step transition. [21] shows vulnerability of bidirectional qZSI due to oscillatory response for an input step change, mainly focused on DC side controllers for oscillation suppression. [22] investigated the coupling effect between qZSI and single order filters, showing that stability and damping is improved by defining the controller parameter safety boundaries.

Interaction of DC and AC side in the voltage fed qZSI can cause instability if left unchecked. The double resonant frequency poses a challenge in controller design, because it produces a much severe effect than conventional VSI. Multiple resonant features due to dynamic interaction of qZSI with AC side are explored in this paper. Oscillations are suppressed using a third order passive damped filter. Harmonics and resonant effects are considered while selecting the size of passive components. Controller response for different design parameters are presented. This study highlights selection of optimal design parameters with sufficient damping to suppress oscillatory response and resonant effects.

Manuscript received on January 24, 2020 ; revised on June 20, 2020 ; accepted on June 23, 2020. This paper was recommended by Associate Editor Yuttana Kumsuwan.

[1]The authors are with the GLA University, Mathura, India.

[2]The author is with the Indira Gandhi National Open University (IGNOU), India.

[†]Corresponding author: arvindyadavpec@gmail.com

Digital Object Identifier 10.37936/ecti-eec.2021191.236885

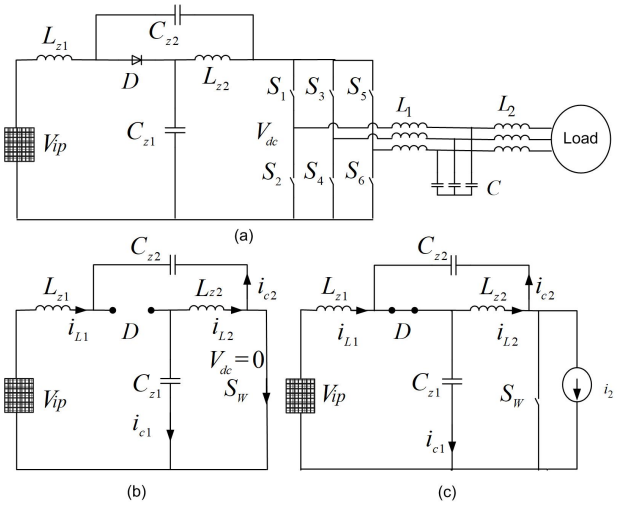

Fig.1: *Equivalent circuit with different modes: (a) voltage fed qZS inverter, (b) shoot-through mode and (c) non shoot-through mode.*

The paper is organized as follows. Section 2 presents DC and AC side dynamic models for control and stability analysis. Combined response of qZSI and AC side is elaborated, then controller design and optimal parameter selection are discussed in Section 3. Section 4 validates the design method and presents results for different parameter design cases. Section 5 concludes the paper.

2. SYSTEM DESCRIPTION AND DYNAMIC MODELING

The system under study consist of a qZS impedance network and a three phase bridge inverter connected to load via a third order LCL filter as shown in Fig. 1. The Impedance network, along with the inverter, constitutes an impedance source inverter. A high boost is achieved in the qZS inverter. The impedance network stores and releases energy during shoot-through (ST) state and non shoot-through (NST) state respectively.

The system dynamic modeling can predict the system transient response, that information is further utilized in designing the closed loop control. In this work, DC and AC sides are modeled separately. Later a combined response is obtained avoiding overlapping of control parameters (i.e modulation index (M) and shoot-through duty ratio (D_s)). The double resonant frequency behavior of the qZS inverter due to presence of additional passive elements in the qZS network is explored.

2.1 DC stage dynamic modeling

A voltage fed qZS passive network with a three phase inverter bridge delivering power to load is shown in Fig. 1. Shoot-through state provides unconventional boosting, and enables buck/boost operations with single stage power conversion. A virtual switch (SW) is used because it allows modeling of DC and AC side separately, then coupled together. Presence of the virtual switch eases modeling and control analysis, and allows separate modeling of DC-DC stage and DC-AC stages. For DC-DC stage modeling, shoot-through and non shoot-through states are considered. An equivalent circuit for ST and NST states is shown in Fig. 1. The state space equations for ST state can be written as $\dot{\mathbf{x}} = \mathbf{A_1}\mathbf{x} + \mathbf{B_1}\mathbf{u}$, where the state vector ($\mathbf{x}$), input vector ($\mathbf{u}$), and output vector ($\mathbf{y}$) are selected as,

$$\mathbf{x} = \begin{bmatrix} i_{L1} \\ i_{L2} \\ v_{C1} \\ v_{C2} \end{bmatrix}, \quad \mathbf{u} = \begin{bmatrix} v_{ip} \\ i_2 \end{bmatrix}, \quad \mathbf{y} = \begin{bmatrix} v_{C1} \\ i_{L1} \end{bmatrix},$$

and

$$\mathbf{A_1} = \begin{bmatrix} \frac{-(r_1+R_2)}{L_{z1}} & 0 & 0 & \frac{1}{L_{z1}} \\ 0 & \frac{-(r_2+R_1)}{L_{z2}} & \frac{1}{L_{z2}} & 0 \\ 0 & \frac{-1}{C_{z1}} & 0 & 0 \\ \frac{-1}{C_{z2}} & 0 & 0 & 0 \end{bmatrix},$$

$$\mathbf{B_1} = \begin{bmatrix} \frac{1}{L_{z1}} & 0 \\ 0 & 0 \\ 0 & 0 \\ 0 & 0 \end{bmatrix}$$

The state space equations for NST state can be written as $\dot{\mathbf{x}} = \mathbf{A_2}\mathbf{x} + \mathbf{B_2}\mathbf{u}$, where

$$\mathbf{A_2} = \begin{bmatrix} \frac{-(r_1+R_1)}{L_{z1}} & 0 & \frac{-1}{L_{z1}} & 0 \\ 0 & \frac{-(r_2+R_2)}{L_{z2}} & 0 & \frac{-1}{L_{z2}} \\ \frac{1}{C_{z1}} & 0 & 0 & 0 \\ 0 & \frac{1}{C_{z2}} & 0 & 0 \end{bmatrix},$$

$$\mathbf{B_2} = \begin{bmatrix} \frac{1}{L_{z1}} & \frac{R_1}{L_{z1}} \\ 0 & \frac{R_2}{L_{z2}} \\ 0 & \frac{-1}{C_{z1}} \\ 0 & \frac{-1}{C_{z2}} \end{bmatrix}$$

The complete model can be expressed as $\dot{\mathbf{x}} = \mathbf{A}\mathbf{x} + \mathbf{B}\mathbf{u}$, where $\mathbf{A} = D_s\mathbf{A_1} + (1 - D_s)\mathbf{A_2}$ and $\mathbf{B} = D_s\mathbf{B_1} + (1 - D_s)\mathbf{B_2}$, D_s is shoot-through duty

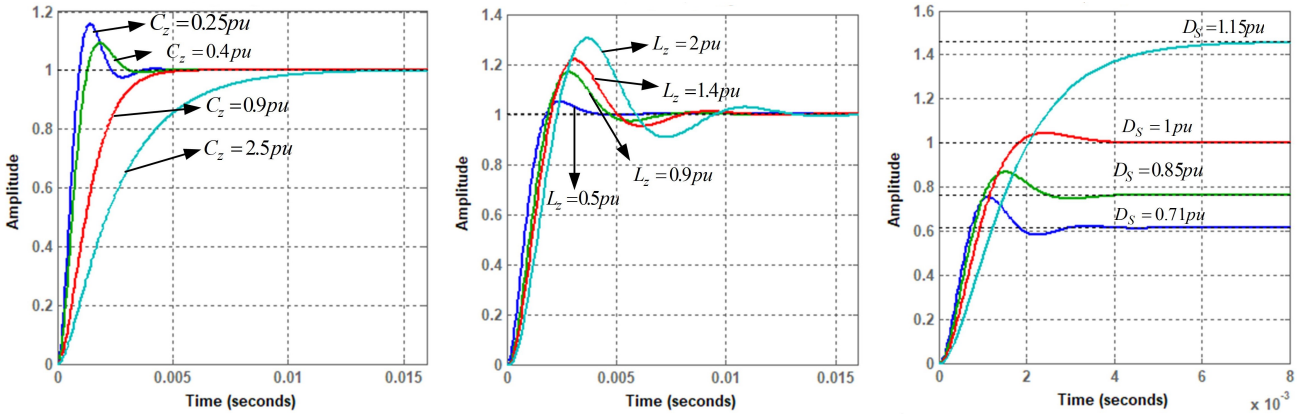

Fig.2: *Step response of Quasi-Z source inverter for parameter sweep.*

$$G_{d_o}^{v_c} = \frac{(V_{C1} + V_{C2} - R_z I_2)(1 - 2D_s) + (I_2 - I_{L1} - I_{L2})(L_z s + r_z + R_z)}{L_z C_z s^2 + C_z(r_z + R_z)s + (1 - 2D_s)^2} \tag{1}$$

ratio described as $D_s = T_o \,/\, T_s$, with shoot-through interval T_o and switching interval $T_s = T_1 + T_o$, where T_1 is non shoot-through interval. For simplification $C_{z1} = C_{z2} = C_z$, $L_1 = L_2 = L_z$, $r_{z1} = r_{z2} = r_z$, $R_{z1} = R_{z2} = R_z$, where

$$\mathbf{A} = \begin{bmatrix} \frac{-(r_z + R_z)}{L_z} & 0 & \frac{D_s - 1}{L_z} & \frac{D_s}{L_z} \\ 0 & \frac{-(r_z + R_z)}{L_z} & \frac{D_s}{L_z} & \frac{D_s - 1}{L_z} \\ \frac{1 - D_s}{C_z} & \frac{-D_s}{C_z} & 0 & 0 \\ \frac{-D_s}{C_z} & \frac{1 - D_s}{C_z} & 0 & 0 \end{bmatrix},$$

$$\mathbf{B} = \begin{bmatrix} \frac{1}{L_z} & \frac{(1 - D_s)R_z}{L_z} \\ 0 & \frac{(1 - D_s)R_z}{L_z} \\ 0 & \frac{D_s - 1}{C_z} \\ 0 & \frac{D_s - 1}{C_z} \end{bmatrix}$$

A small signal model is obtained by introducing perturbation in average model. Dynamic influence on the DC side is given by capacitor voltage to the shoot-through duty ratio transfer function as shown in Eq. (1). The effect of parameter variation (L_z, C_z and D_s) was investigated on open loop transfer function ($G_{d_o}^{v_c}$), and a summary of parameter variations on system dynamics is shown in Table 1. The characteristic equation (Eq. (1)) indicates a resonance frequency. However, load and parasitic resistance can diminish the resonant effect of the impedance network of the qZS inverter. Steady state values can be obtained by setting $\mathbf{Ax} + \mathbf{Bu} = 0$, DC steady state values must also satisfy Eq. (2). Peak DC link voltage at the inverter is shown in Eq. (3). Output voltage of the inverter will be given by Eq. (4), where $\hat{V}_2$ is the phase peak and M is the modulation index.

$$I_{L1} = I_{L2}, \quad V_{c1} = \frac{1 - D_s}{1 - 2D_s} v_{ip} = V_{c2} + v_{ip} \tag{2}$$

$$\hat{V}_{dc} = \frac{1}{1 - 2D_s} v_{ip} = V_{c1} + V_{c2} \tag{3}$$

$$\hat{V}_2 = \frac{M}{2} \hat{V}_{dc} = \frac{1}{1 - 2D_s} \frac{M}{2} v_{ip} \tag{4}$$

From Eq. (4), it is evident that output voltage of inverter is having two degrees of freedom, M and D_s. Therefore it can be controlled by adjusting control parameters M and d_s. During steady state, $d_s = D_s$, so the control parameters can be integrated using various modulation techniques [23–26]. Here simple boost control was used.

With the help of a pole-zero map, examining step response considering parameter variation helps in optimum size selection of passive elements (L_z, C_z), as they influence the system dynamics and can make closed loop control more complex. DC side response for parameter variation is shown in Fig. 2. Table 1 summarizes the impact of parameter variation on qZS inverter system dynamics.

2.2 AC stage dynamic modeling

A voltage source PWM inverter is a harmonic generator. A filter is required to comply with strict grid codes. A third order LCL filter is connected to the load side. LCL filters are capable of harmonic attenuation at even low frequencies, but the problem of resonance and stability should be dealt carefully [27, 28]. Fig. 3 represents the per phase block diagram

Table 1: *Summary of impact of parameter variation on qZSI system dynamics using Pole-Zero map.*

Parameter (variation)	Symbol	Effect on Pole-Zero map	Impact on system dynamics
Inductance (increasing)	L_z	Conjugate poles & real poles shift towards the vertical axis, RHP zero shift towards the vertical axis	• increment in system settling time • reduction in the system damping • reduction in natural frequency • increment in NMP undershoot
Capacitance (increasing)	C_z	Conjugate poles shift closer to horizontal axis, RHP zero remains constant	• increment in system settling time • increment in system damping • reduction in natural frequency
Shoot-through duty ratio (increasing)	D_s	Conjugate poles shift closer to horizontal axis, RHP zeros shift towards the vertical axis	• increment in system settling time • reduction in natural frequency • increment in NMP undershoot
Inductor parasitic resistance (increasing)	R_z	Conjugate poles shift towards the horizontal axis & move away from the vertical axis, RHP zeros shift closer to vertical axis	• increment in system settling time • increment in the system damping • introduces ripples in inductor voltage • increment in NMP undershoot
Capacitor ESR (increasing)	r_z	Conjugates poles shift towards the horizontal axis & move away from the vertical axis, RHP zeros shift closer to vertical axis	• reduction in system settling time • increment in the system damping • introduces ripples in capacitor current • increment in NMP undershoot

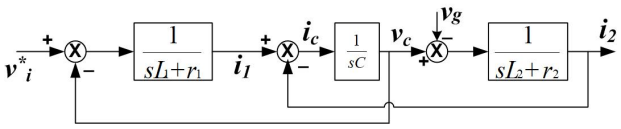

Fig.3: *Per phase block diagram representation of a third order filter.*

of an LCL filter considering parasitic resistance of an inverter side inductor (L_1, r_1) and a grid side inductor (L_2, r_2). Here the inverter is treated as a harmonic generator. The grid supply contains only positive sequence component, which means it can be treated as short-circuit while performing harmonic analysis. The overall control structure incorporating AC side and DC side control layout is shown in Fig. 4. With the assumption of a stiff grid, the transfer function for the grid side current (i_2) to the inverter side voltage (v_i) at non fundamental frequencies is given in Eq. (5). The absence of parasitic resistance represents the system worst damping performance. In Eq. (6), is given the resonance frequency (ω_{res}) for LCL filter.

$$\frac{i_2(s)}{v_i(s)} = \frac{1}{s^3 C L_1 L_2 + s(L_1 + L_2)} \tag{5}$$

$$\omega_{res} = \sqrt{\frac{L_1 + L_2}{C L_1 L_2}} \tag{6}$$

Due to insufficient damping, the system shown in Fig. 3 depicts stability issues with large oscillations. An adequate damping can be obtained using an optimum damping resistance (r_d) in series with the filter capacitor (C). This paper also presents the performance of a third order LCL filter (with and without a damping resistor). A single phase block representation of the LCL filter considering all

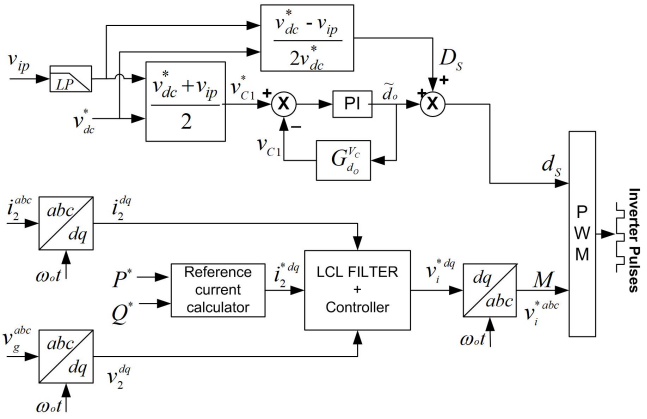

Fig.4: *Control block diagram for a qZSI connected system.*

parasitic and damping resistance is shown in Fig. 5. The system can be defined using Eq. (7).

$$\begin{aligned} L_1 \frac{di_1}{dt} &= v_i - v_c - i_1 r_1 - i_c r_d \\ L_{2g} \frac{di_2}{dt} &= v_c + i_c r_d - i_2 r_{2g} - v_g \\ C \frac{dv_c}{dt} &= i_1 - i_2 = i_c \end{aligned} \tag{7}$$

3. OPTIMAL PARAMETER SELECTION & CONTROLLER DESIGN

The input to the qZS inverter connected system can be fed from a renewable energy source. Most renewable sources are intermittent in nature. They produces low output which can be boosted to a required level. Grid connected converters are bound to comply with frequency, voltage magnitude, and harmonic attenuation. On the DC side, the system

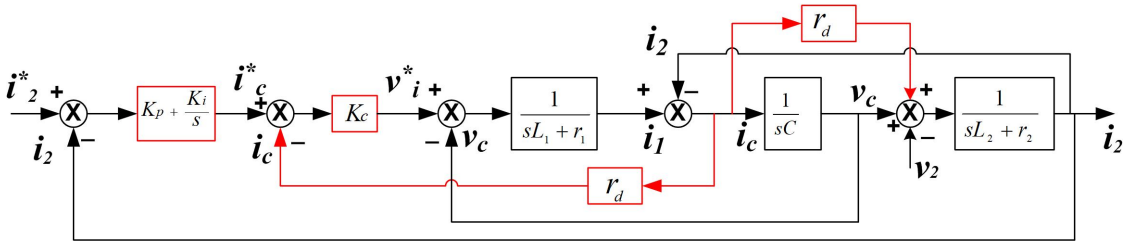

Fig.5: *Per phase control block diagram representation of a third order damped filter.*

response is governed by the size of passive elements. These components are important when designing a closed loop control. Instead of DC link voltage, capacitor voltage is selected as controller feedback. Input voltage is sensed directly, whereas reference for the capacitor voltage is evaluated indirectly, as shown in Fig. 5. A PI regulator is used to regulate the duty ratio (d_s) so that v_{dc} is kept constant.

The open loop transfer function G_{cdo} and closed loop transfer function G_{cdc} are given in Eqs. (8) and (9) respectively.

$$G_{cdo} = \frac{v_{c1}}{d_o} = \frac{a_1 s + a_0}{b_2 s^2 + b_1 s + b_0} \tag{8}$$

where

$$a_0 = (r_z{+}R_z)(I_2{-}I_{L1}{-}I_{L2}){+}(V_{C1}{+}V_{C2}{-}RI_2)(1{-}2D_s),$$
$$a_1 = L_z(I_2 - I_{L1} - I_{L2}), \quad b_0 = (1-2D_s)^2,$$
$$b_1 = C_z(r_z + R_z), \quad b_2 = L_z C_z.$$

$$G_{cdc} = \frac{v_{c1}}{v_{c1}^{\star} - v_{c1}} = \frac{A_2' s^2 + A_1' s + A_0'}{B_3' s^3 + B_2' s^2 + B_1' s + B_0'} \tag{9}$$

where $A_0' = a_0 k_2$, $A_1' = k_1 a_0 + k_2 a_1$, $A_2' = a_1 k_1$, $B_0' = 0$, $B_1' = k_1 a_0 {+} k_2 a_1 {+} b_0 {+} k_2 a_0$, $B_2' = k_1 a_1 {+} b_1$, $B_3' = b_2$.

The range of PI parameters for stable operation is obtained using Routh's stability criteria on the characteristic equation of G_{cdc}. The second order equation $s^2 + 2\xi\omega_n s + \omega_n^2$ can be correlated with the characteristic equation of G_{cdo}. It provides the natural frequency ω_n and damping ratio ξ, hence it guides passive component size selection of the qZS inverter. A tradeoffs between settling time, system damping, natural frequency and non-minimum phase undershoot will yield the optimal size of qZS inverter passive elements. The voltage controller shown in Fig. 6 will respond to the step change in v_{ip}. The qZS network parameters obtained for $\xi = 1/\sqrt{2}$ are $L_z = 390\,\mu$H, $C_z = 280\,\mu$F. They are treated as base values for parameter variation with $d_s = 0.35$. Applying Routh-Hurwitz stability criteria to the characteristic equation of the transfer function obtained in Eq. (9) gives values for PI controller gains $k_1 = 0.36 \times 10^{-3}$ and $k_2 = 0.076$. By setting

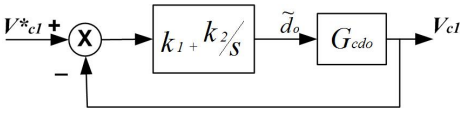

Fig.6: *DC side voltage controller.*

$|G_{cdo}G_{cdc}| = 1$, a cross over frequency is obtained. The gain margin obtained after compensation is 20 dB. The resonant feature at DC side is diminished by parasitic resistance of the qZS inverter passive components. The voltage controller loop on the DC side enables tracking of $v_{c1}^{\star}$. A steeper descending slope in the bode plot indicates good tracking with reduced steady state error, decreased oscillations, and improved stability. It is also visible in the time domain response (Fig. 14). As the DC link voltage is pulsating with high magnitude, therefore it will not be considered for controller feedback, since it can make controller output oscillating, causing stability problems for DC side input transition. Capacitor voltage is considered for controller feedback to make DC link voltage constant.

A third order filter uses small passive elements and provides better harmonic and ripple attenuation over a high frequency range. However, the resonance effect becomes severe if it is not suppressed with sufficient damping. Here a damping resistor r_d is employed in series with a filter capacitor C. Considering parasitic resistance and the damping resistor, Eq. (5) must be modified as

$$\frac{i_2(s)}{v_i(s)} = \frac{A_1 s + A_0}{B_3 s^3 + B_2 s^2 + B_1 s + B_0} \tag{10}$$

where $A_0 = 1$, $A_1 = Cr_d$, $B_0 = r_2 + r_1$, $B_1 = r_1 C(r_2 + r_d) + Cr_2 r_d + L_1 + L_2$, $B_2 = C(r_1 L_2 + r_2 L_1 + r_d(L_1 + L_2))$, $B_3 = CL_1 L_2$.

With slight modification, Eq. (6) can be written as Eq. (11). With an assumption of a stiff grid, the total inductance $L_{sum} = L_1 + L_2$, ratio $\eta = L_2 \,/\, L_1$ and ratio $f_r = f_{sw} \,/\, f_{res}$, where f_{sw} is the switching frequency of PWM.

$$L_{sum} C = \frac{(1+\eta)^2}{\eta} \frac{f_r^2}{4\pi^2 f_{sw}^2} \tag{11}$$

One of the main goals is to design the LCL filter with minimum passive component size without com-

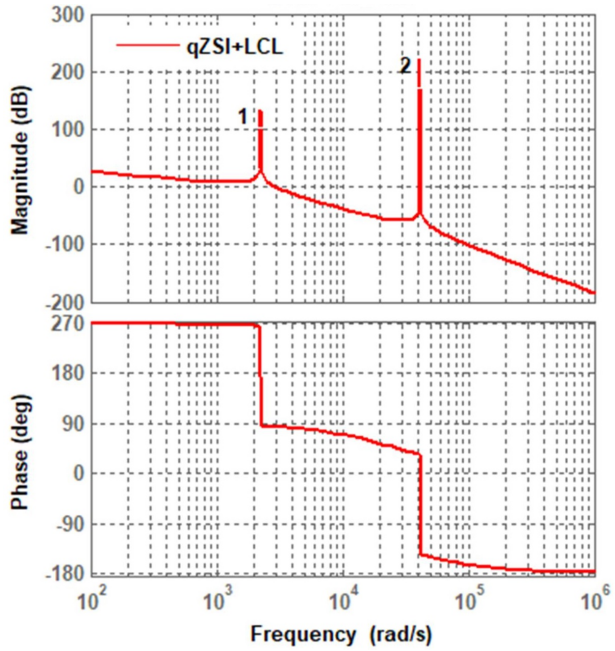

Fig.7: *Frequency response of qZS inverter connected system.*

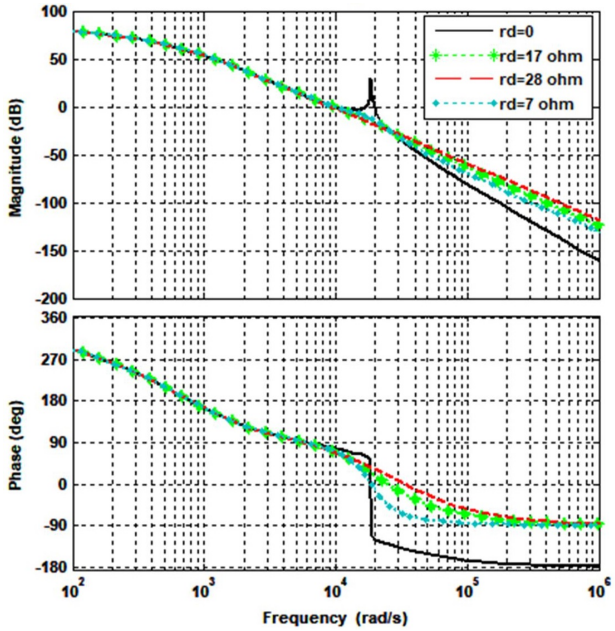

Fig.8: *Effect of damping on frequency response of coupled (qZSI+LCL) structure.*

promising attenuation and system stability. Eq. (11) will make obtaining the optimum values of η and f_r which results in the minimum $L_{sum}C$ product. At a given resonance frequency, minimum product of $L_{sum}C$ can be determined by differentiating Eq. (11). The situation gets worse when both DC and AC sides are coupled to get overall system response, as shown in Fig. 7. The frequency response of qZS inverter system of Fig. 1 is shown in Fig. 8, with negligible

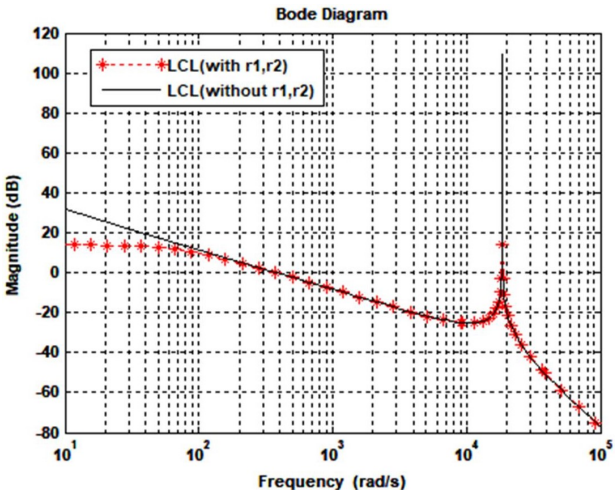

Fig.9: *Effect of parasitic resistance on magnitude plot of LCL filter.*

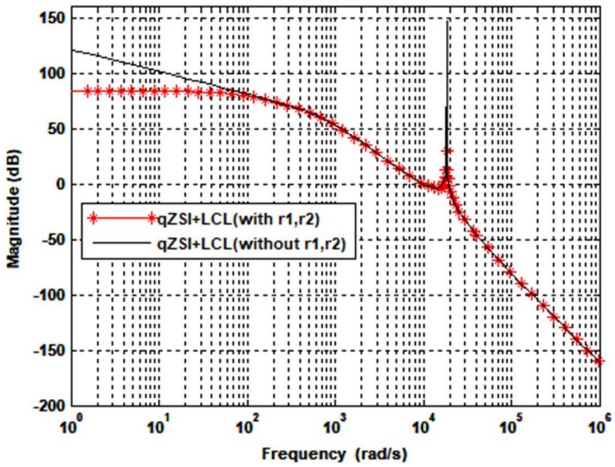

Fig.10: *Frequency response of coupled (qZSI+LCL) structure.*

parasitic resistances. Two resonant peaks are visible for the qZS connected system as shown in Fig. 7. The qZS inverter contributes peak 1, whereas third order filter contributes peak 2. The third order LCL filter frequency response is shown in Fig. 9, and qZS inverter response considering parasitic resistance (r_1, r_2) is shown in Fig. 10. Peak 1 is absent, whereas peak 2 is damped due to inherent damping caused by AC side filter. AC side parasitic resistance (r_1, r_2) has reduced the magnitude of peak 2 from 140 db to 70 db as shown in Fig. 10. Even with inherent damping, high resonance peak is obtained.

Magnitude at resonance is further reduced with the introduction of r_d to the LCL filter. The characteristic equation Eq. (10) can be used as a guide for finding the optimum value of r_d. For different values of r_d, response of Eq. (10) is shown in Fig. 8. The effect of the choice of damping resistor is presented in Table 2. The optimum value for $\xi = 0.707$ is 17 Ω. The corresponding inverter side

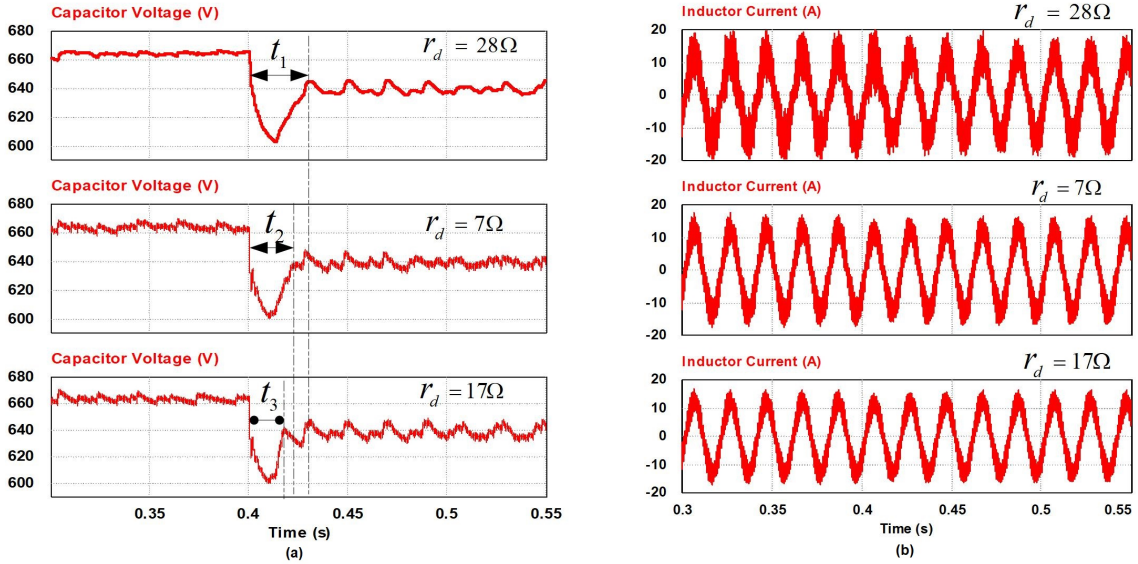

Fig.11: *Waveforms for different r_d values: (a) capacitor voltage (v_{c1}) and (b) inverter side current i_1.*

current THD is 21%, the corresponding capacitor voltage (v_{c1}) settling time is 0.018 s. Fig. 11 shows the inverter side current (i_1) and capacitor voltage (v_{c1}) waveform for $\xi = 0.3$, 0.707 and 1.2. The choice of r_d directly affects the settling time, and thus system must be underdamped with reduced oscillation.

On the AC side, the *dq* axis control structure is obtained to avoid quadrature and direct axis components interaction. An *abc* to *dq* transformation is used in synchronous reference frame. State space equation in *dq* format can be written as,

$$\begin{aligned}
L_1\frac{di_1^d}{dt} &= v_i^d - v_c^d - i_1^d r_1 - i_c^d r_d + \omega L_1 i_1^q \\
L_{2g}\frac{di_2^d}{dt} &= v_c^d + i_c^d r_d - i_2^d r_{2g} - v_g^d + \omega L_{2g} i_2^q \\
C\frac{dv_c^d}{dt} &= i_c^d + \omega C v_c^q \\
L_1\frac{di_1^q}{dt} &= v_i^q - v_c^q - i_1^q r_1 - i_c^q r_d - \omega L_1 i_1^d \\
L_{2g}\frac{di_2^q}{dt} &= v_c^q + i_c^q r_d - i_2^q r_{2g} - v_g^q - \omega L_{2g} i_2^d \\
C\frac{dv_c^q}{dt} &= i_c^q - \omega C v_c^d
\end{aligned} \tag{12}$$

The AC side *dq* control structure is shown in Fig. 4. The dual current loops with an inscribed voltage loop enable control objective. The inner current (i_c) loop is made faster than the outer current (i_2) loop by suitably selecting PI controller gains. The voltage loop inscribed in the inner current loop provides damping. Using Eqs. (10) and (11) with Table 2, base parameters for the third order filter based qZS inverter system are given in Table 3.

Table 2: *Summary of variation of r_d on qZS inverter connected system.*

Damping resistor (r_d)	Damping factor (ξ)	Inverter current(i_1) THD	Settling time v_{c1}
7 Ω	0.3	23%	0.025 s
17 Ω	0.707	21%	0.018 s
28 Ω	1.2	31%	0.03 s

On the DC side, the voltage controller provides the shoot-through duty ratio. The modulation index M is obtained from the dual current loop control on the AC side, as shown in Fig. 4. Finally control parameters (d_s and M) are integrated using simple boost pulse width modulation.

4. RESULT AND DISCUSSION

This section verifies the effectiveness of design parameters for qZS inverter passive components, the LCL filter, and the DC and AC side controllers. The designed parameters are summarized in Table 3. Compared to a conventional PWM inverter, the qZS inverter has two degrees of freedom, provides high boost, and permits short circuiting of switches on same leg. For a disturbance on the input side, the effectiveness of our control method is evaluated. Source side disturbance is modeled as a step change, and with our controller action, disturbance is mitigated efficiently. The performance of the small signal model is verified using a PSIM/MATLAB/Simulink, a dSPACE 1104 control board, and a three phase inverter which uses SKM100GB125DN IGBT module. A CN240610

Table 3: *Base parameters for third order passive damped filter based qZS inverter system*

Elements	Parameter	Value
qZS Inverter	Inductance (L_z) Capacitance (C_z) Parasitic resistance (r_z, R_z) Switching frequency	390 μH 280 μF 0.47 Ω, 0.03 Ω 8 kHz
LCL Filter	Inverter side inductance (L_1, r_1) Filter capacitance (C) Damping resistor (r_d) Grid side inductance (L_2, r_2)	1.3 mH, 0.1 Ω 4.5 μF 17 Ω 1.3 mH, 0.1 Ω
Load	Line frequency Nominal power Load current/phase Grid voltage/phase	50 Hz 5 kW 9 A 230 V

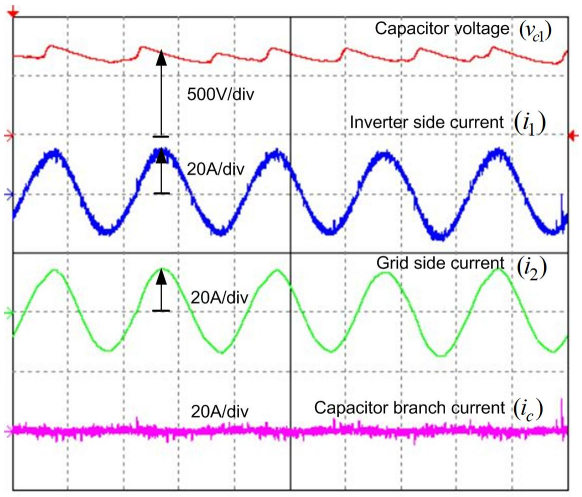

Fig.12: *Observed waveforms for Case I, showing capacitor voltage (v_{c1}), inverter side current (i_1), load current (i_2) and capacitor branch current (i_c).*

Table 4: *Summary of comparative assessment for cases I and II.*

Parameter	Case I	Case II
ratio η	1.2 pu	1 pu
f_{res}, ratio f_r	0.8pu, 3.4	1 pu, 2.72
step change in V_{ip}	100% to 83%	100% to 83%
Inverter current (i_1) THD	29%	21%
capacitor voltage (v_{c1}) ripple	12%	2%
Load voltage (v_2) THD	9%	3.6%
LCL Filter size	1.57 pu	1 pu

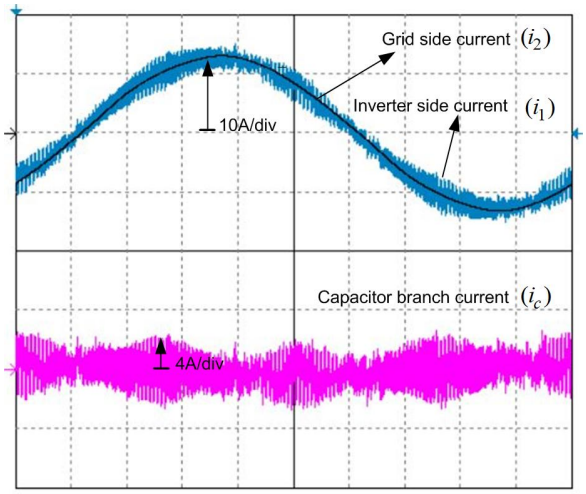

Fig.13: *Observed waveforms in an open loop condition for Case II, showing results for inverter side current (i_1), load current (i_2) and capacitor branch current (i_c).*

power diode is used. Reduced input at source side leads to reduced DC link voltage (v_{dc}). The current and voltage magnitude get altered at load side, but can be corrected with controller action. DC side voltage controller ensures constant DC link voltage by generating required shoot-through duty pulses. The dual current loop provides necessary voltage modulation on the AC side.

The behavior of a qZS inverter is not as straight forward as that of a conventional PWM inverter due to the presence of additional passive elements in a qZS network. The system response gets more severe due to the presence of additional passive components. Inherent damping is caused due to parasitic resistance, but that is insufficient to guarantee a well damped system, as shown in Figs. 8 and 10. Moreover, the poor filter design will vain all efforts. The overall control structure integrating DC and AC side controllers is shown in Fig. 4. With introduction of a damping resistor, a left half plane zero is introduced in the filter transfer function. This makes step response faster by reducing rise time and peak time, but overshoot is increased. The value of r_d must be carefully selected for effective damping.

This study presents controller response in two cases. Case I includes a poorly designed filter. Case II includes a well designed filter. System parameters for case I are $L_1 = 1.2$ pu, $C = 1.2$ pu and $\eta = 1.2$. The load parameters are unchanged. Case I results captured in the oscilloscope are shown in Fig. 12. Capacitor voltage (v_{c1}) has sustained oscillations with a ripple of 12%, which is reflected at inverter side also. This results in a much distorted current (i_1) and voltage (v_2). The reference generated by the controllers also oscillates. As a result, capacitor

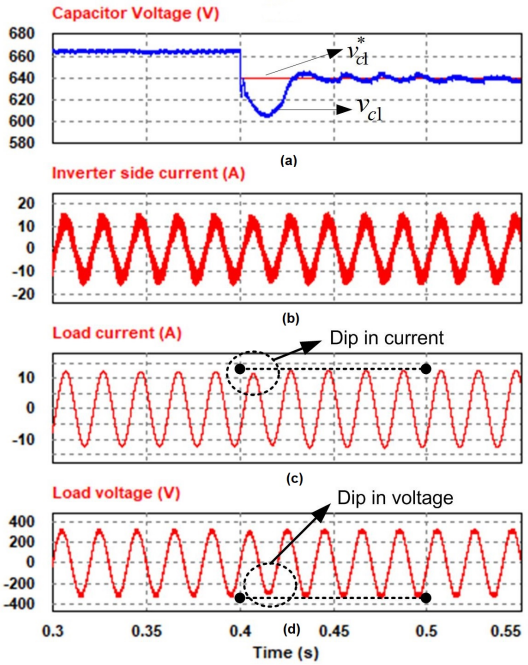

Fig.14: *Simulation result for a step change in V_{ip} showing: (a) capacitor voltage (v_{c1}), (b) inverter side current (i_1), (c) load current (i_2) and (d) load voltage (v_2).*

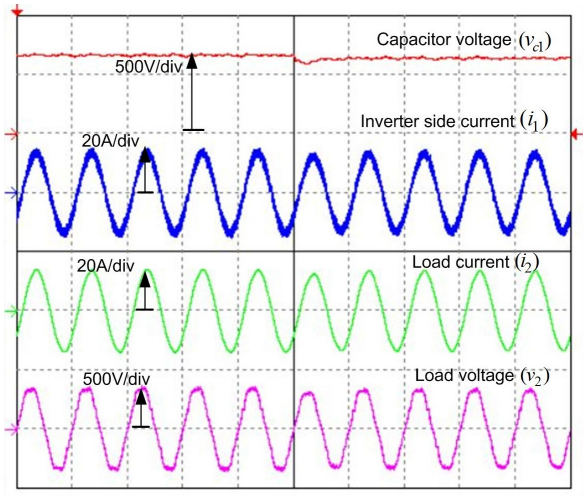

Fig.15: *Observed waveforms for a step change in Case II, showing results for capacitor voltage (v_{c1}), inverter side current (i_1), load current (i_2) and load voltage (v_2).*

voltage (v_{c1}) after correction also oscillates. The filter is unable to improve the harmonic distortion. Thus this filter fails in the prime objective only. The overall size of filter defined by $L_{sum}C$ product has increased 1.57 fold, the capacitor voltage settling time increased, and the load current and voltage harmonic content increased. Table 4 presents the summarized result for case I.

For a well designed plant, the controller action guarantees disturbance rejection. In case II, parameters selected are shown in Table 3. Various waveforms for case II are shown in Fig. 13 for open loop condition. Under normal operating conditions, 300 V is sensed on the input side by a voltage sensor. The shoot-through duty ratio is 0.35, the grid current 9 A for a load power of 5 kW, and the required DC link voltage ($v_{dc}^\star$) is 1030 V. A step change from 100% to 83% in V_{ip} is forced at 0.4 s. The sensed input voltage (v_{ip}), alongwith DC link voltage ($v_{dc}^\star$), is used to estimate the steady state shoot-through duty ratio (D_s) and required capacitor voltage ($v_{c1}^\star$). The error ($v_{c1}^\star$-v_{c1}) is forwarded to a Proportional-Integral controller to produce the correction in the shoot-through duty ratio. A dip in capacitor voltage ($v_{c1}^\star$) is visible in Figs. 14 and 15. This is effectively tracked by controller action on the DC side. An equivalent duty-ratio (d_s) is obtained by combining d_o and D_s as shown in Fig. 4. On the AC side, load voltage v_2 and current i_2 is sensed. Reference current is generated by required active and reactive power. A dual current loop consisting of outer current loop (i_2) and inner current loop (i_c), as shown in Fig. 5, is used to generate the required inverter voltage (v_i). Newly calculated M and d_s are integrated using simple boost control.

A voltage loop inscribed within the inner current loop helps in obtaining a damped response. A reduced peak in load current (i_2) and voltage (v_2) is visible for one cycle. With help of AC and DC controller actions, i_2 and v_2 are maintained at their required values as shown in Figs. 14 and 15. When compared with case I, a reduced capacitor voltage ripple of 2% is obtained. A well designed third order passive damped filter decreases current and voltage harmonic content, improves capacitor voltage ripple, and decreases filter size. Table 4 presents the summarized results for both cases.

5. CONCLUSION

This paper investigates the qZS inverter for a third order passive filter. A virtual switch is used to separate DC and AC stage dynamic models. Various transfer functions for the DC and AC sides have been derived. The impact of parameter variation of qZS network passive elements is summarized. Optimal parameters for DC side network, the LCL filter, and the controllers are selected using derived closed loop transfer functions. The need for external damping in the third order filter has been highlighted because the inherent damping is insufficient for a stable system with a stable controller response. Magnitude and frequency response are analyzed for the LCL connected qZS inverter system. The impact of a damping resistor on stability, harmonic attenuation, and transient response was evaluated. For verification of the design parameters and controller performance,

PSIM/MATLAB/Simulink models are used. Specifically, the IGBT module (SKM100GB125DN) with power diode (CN240610) was used.

A voltage controller on the DC side, a dual current loop control, along with an inscribed voltage loop on the AC side, helped achieve stable response with efficient damping. Magnitude plots, frequency plots, gain and phase margins and Routh-Hurwitz stability criteria were used for controller parameter design. A reduction in filter size, high harmonic attenuation, improved damping, and low capacitor voltage ripple was achieved using a third order passive damped filter. This study also compared controller response for poorly and optimally chosen design parameters. The results validated the design guidelines for a dual current loop control for a voltage fed qZS inverter feeding power via a third order filter. We recommended external damping for further performance improvement.

ACKNOWLEDGEMENT

This research has been supported by GLA University, Mathura, India. Authors are thankful to GLA University and the Department of Electrical Engineering for providing access to dSPACE 1104 and the Solar Energy Lab.

References

[1] F. Z. Peng, "Z-Source Inverters," in *Wiley Encyclopedia of Electrical and Electronics Engineering*, J. G. Webster, Ed., John Wiley & Sons, 2017, pp. 1–11.

[2] Y. P. Siwakoti, F. Z. Peng, F. Blaabjerg, P. C. Loh and G. E. Town, "Impedance-Source Networks for Electric Power Conversion Part I: A Topological Review," *IEEE Transactions on Power Electronics*, vol. 30, no. 2, pp. 699–716, 2015.

[3] Y. P. Siwakoti, F. Blaabjerg and P. C. Loh, "New Magnetically Coupled Impedance (Z-) Source Networks," *IEEE Transactions on Power Electronics*, vol. 31, no. 11, pp. 7419–7435, 2016.

[4] W. Qian, F. Z. Peng and H. Cha, "Trans-Z-Source Inverters," *IEEE Transactions on Power Electronics*, vol. 26, no. 12, pp. 3453–3463, 2011.

[5] J. Anderson and F. Z. Peng, "A Class of Quasi-Z-Source Inverters," in *2008 IEEE Industry Applications Society Annual Meeting*, 2008, pp. 1–7.

[6] Q. Tran, T. Chun, J. Ahn and H. Lee, "Algorithms for Controlling Both the DC Boost and AC Output Voltage of Z-Source Inverter," *IEEE Transactions on Industrial Electronics*, vol. 54, no. 5, pp. 2745–2750, 2007.

[7] A. Yadav and S. Chandra, "Single stage high boost Quasi-Z-Source inverter for off-grid photovoltaic application," in *2020 International Conference on Power Electronics & IoT Applications in Renewable Energy and its Control (PARC)*, 2020, pp. 257–262.

[8] A. Badhoutiya and A. Yadav, "Boost control for PV applications using impedance source inverter," in *2017 2nd IEEE International Conference on Recent Trends in Electronics, Information & Communication Technology (RTEICT)*, 2017, pp. 1967–1970.

[9] A. Yadav, S. Chandra, V. Deolia and S. Agrawal. "Z source inverter application and control for decentralized photovoltaic system," in *2017 3rd International Conference on Condition Assessment Techniques in Electrical Systems (CATCON)*, 2017, pp. 52–57.

[10] J. Liu, J. Hu and L. Xu, "Dynamic Modeling and Analysis of Z Source Converter–Derivation of AC Small Signal Model and Design-Oriented Analysis," *IEEE Transactions on Power Electronics*, vol. 22, no. 5, pp. 1786–1796, 2007.

[11] Y. Li, S. Jiang, J. G. Cintron-Rivera and F. Z. Peng, "Modeling and Control of Quasi-Z-Source Inverter for Distributed Generation Applications," *IEEE Transactions on Industrial Electronics*, vol. 60, no. 4, pp. 1532–1541, 2013.

[12] A. Yadav, V. Deolia and S. Agrawal, "Influence of parasitic resistance on dynamic response of a Quasi-Z-Source connected system," in *2020 International Conference on Power Electronics & IoT Applications in Renewable Energy and its Control (PARC)*, 2020, pp. 220-225.

[13] W. Wu, Y. He, T. Tang and F. Blaabjerg. "A New Design Method for the Passive Damped LCL and LLCL Filter-Based Single-Phase Grid-Tied Inverter," *IEEE Transactions on Industrial Electronics*, vol. 60, no. 10, pp. 4339–4350, 2013.

[14] Y. Tang, P. C. Loh, P. Wang, F. H. Choo and F. Gao, "Exploring Inherent Damping Characteristic of LCL-Filters for Three-Phase Grid-Connected Voltage Source Inverters," *IEEE Transactions on Power Electronics*, vol. 27, no. 3, pp. 1433–1443, 2012.

[15] M. Said-Romdhane, M. Naouar, I. Belkhodja and E. Monmasson, "An Improved LCL Filter Design in order to Ensure Stability without Damping and Despite Large Grid Impedance Variations," *Energies*, vol. 10, no. 3, p. 336, 2017.

[16] R. Peña-Alzola, M. Liserre, F. Blaabjerg, M. Ordonez and Y. Yang, "LCL-Filter Design for Robust Active Damping in Grid-Connected Converters," *IEEE Transactions on Industrial Informatics*, vol. 10, no. 4, pp. 2192–2203, 2014.

[17] Y. Liu, B. Ge, H. Abu-Rub and F. Z. Peng, "An Effective Control Method for Quasi-Z-Source Cascade Multilevel Inverter-Based Grid-Tie Single-Phase Photovoltaic Power System," *IEEE Transactions on Industrial Informatics*, vol. 10, no. 1, pp. 399–407, 2014.

[18] N. Singh and S. K. Jain, "A novel strategy for

indirect control of peak dc-link voltage of grid-connected qZS inverter fed through renewable energy sources," *Electrical Engineering*, vol. 102, pp. 611–625, 2020.

[19] Z. Rymarski and K. Bernacki, "Influence of Z-source output impedance on dynamic properties of single-phase voltage source inverters for uninterrupted power supply," *IET Power Electronics*, vol. 7, no. 8, pp. 1978–1988, 2014.

[20] P. C. Loh, C. J. Gajanayake, D. M. Vilathgamuwa and F. Blaabjerg, "Evaluation of Resonant Damping Techniquesfor Z-Source Current-Type Inverter," *IEEE Transactions on Power Electronics*, vol. 23, no. 4, pp. 2035–2043, 2008.

[21] F. Guo, L. Fu, C. Lin, C. Li and J. Wang, "Small signal modeling and controller design of a bidirectional Quasi-Z-Source inverter for electric vehicle applications," in *2012 IEEE Energy Conversion Congress and Exposition (ECCE)*, 2012, pp. 2223–2228.

[22] Y. Shi, T. Kayiranga, Y. Li and H. Li, "Exploring the LCL Characteristics in GaN-Based Single-L Quasi-Z-Source Grid-Tied Inverters," *IEEE Transactions on Industrial Electronics*, vol. 64, no. 10, pp. 7758–7768, 2017.

[23] M. Shen, J. Wang, A. Joseph, F. Z. Peng, L. M. Tolbert and D. J. Adams, "Constant boost control of the Z-source inverter to minimize current ripple and voltage stress," *IEEE Transactions on Industry Applications*, vol. 42, no. 3, pp. 770–778, 2006.

[24] C. Charumit and V. Kinnares, "Discontinuous SVPWM Techniques of Three-Leg VSI-Fed Balanced Two-Phase Loads for Reduced Switching Losses and Current Ripple," *IEEE Transactions on Power Electronics*, vol. 30, no. 4, pp. 2191–2204, 2015.

[25] M. S. Diab, A. A. Elserougi, A. M. Massoud, A. S. Abdel-Khalik and S. Ahmed, "A Pulsewidth Modulation Technique for High-Voltage Gain Operation of Three-Phase Z-Source Inverters," *IEEE Journal of Emerging and Selected Topics in Power Electronics*, vol. 4, no. 2, pp. 521–533, 2016.

[26] F. Z. Peng, M. Shen and Z. Qian, "Maximum boost control of the Z-source inverter," *IEEE Transactions on Power Electronics*, vol. 20, no. 4, pp. 833–838, 2005.

[27] S. Jayalath and M. Hanif, "Generalized LCL-Filter Design Algorithm for Grid-Connected Voltage-Source Inverter," *IEEE Transactions on Industrial Electronics*, vol. 64, no. 3, pp. 1905–1915, 2017.

[28] J. Dannehl, C. Wessels and F. W. Fuchs, "Limitations of Voltage-Oriented PI Current Control of Grid-Connected PWM Rectifiers with LCL Filters," *IEEE Transactions on Industrial Electronics*, vol. 56, no. 2, pp. 380–388, 2009.

Arvind Yadav received his B.Tech. from the Himachal Pradesh University, India, in 2007, and his M.E. from the Punjab Engineering College, Chandigarh, India, in 2013. He is currently working as an Assistant Professor and also pursuing his Ph.D. in the Department of Electrical Engineering, GLA University, Mathura, India. His research interest includes power electronics converters, electric drives, grid integration technologies, and application of power electronics in sustainable renewable energy.

Vinay Kumar Deolia is working as a Professor and is Head of the Department of Electronics and Communication Engineering, Institute of Engineering and Technology, GLA University, Mathura, India. He completed his Ph.D. in Backstepping control from NIT, Allahabad, India. His areas of interest include nonlinear control systems, IDMA, power electronics converter control, and other recent trends in technology. He has more than 20 years of experience in teaching and research.

Sanjay Agrawal received his B.Tech. from MMM Gorakhpur, India, his M.Tech. from UP technical University Lucknow, India, and his Ph.D. from IIT, Delhi, India. He was a Post-Doctoral Fellow SMERC, University of California, Los Angeles, CA, USA. Currently he is working as an Associate Professor in the Institute of Engineering and Technology, Indira Gandhi National Open University (IGNOU), India. His research interest are Solar photovoltaic systems, hybrid PV/T, CO_2, Exergy analysis, and Carbon trading. He has published more than 20 research papers and attended many workshops in the area of renewable energy. He has worked for two sponsored projects, and has been invited as a guest for expert talk in various prestigious institutes. He has guided 10 post graduate thesis and 3 Ph.D. thesis, currently 6 more Ph.D thesis are in progress. He is a professional member of Institution of Engineers and Institute of Electrical and Electronics Engineers.